

Phase Diagrams for Spin-1 Bosons in an Optical Lattice

Ming-Chiang Chung and Sungkit Yip

Institute of Physics, Academia Sinica, Taipei 11529, Taiwan

(Dated: February 12, 2022)

In this paper, the phase diagrams of a polar spin-1 Bose gas in a three-dimensional optical lattice with linear and quadratic Zeeman effects both at zero and finite temperatures are obtained within mean-field theory. The phase diagrams can be regrouped to two different parameter regimes depending on the magnitude of the quadratic Zeeman effect Q . For large Q , only a first-order phase transition from the nematic (NM) phase to the fully magnetic (FM) phase is found, while in the case of small Q , a first-order phase transition from the nematic phase to the partially magnetic (PM) phase, plus a second-order phase transition from the PM phase to the FM phase is obtained. If a net magnetization in the system exists, the first-order phase transition causes a coexistence of two phases and phase separation: for large Q , NM and FM phases and for small Q , NM and PM phases. The phase diagrams in terms of net magnetization are also obtained.

PACS numbers: 37.10.Jk, 03.75.-b, 75.25.+z

I. INTRODUCTION

The study of cold atoms in optical lattices has captured a lot of recent attention. A primary motivation is to study the strongly repulsive (two spin species) Fermi Hubbard model in the regime of close to one atom per lattice site in two dimension, a system which is believed by many to capture the most essential physics of the high temperature oxide superconductors [1]. Much progress has already been made towards this goal, in particular the Mott insulating phase in three dimension has already been obtained [2, 3]. However, the expected anti-ferromagnetic Neel ordering has not yet been reported, perhaps due to the difficulty in cooling fermions.

On the other hand, there are also substantial interests in studying Bosons with spins in the Mott insulating regime in an optical lattice. There have already been quite a number of experimental studies on spinor Bose-Einstein condensates (without optical lattice) [4, 5, 6, 7, 8, 9]. Mott insulating state of Bosons with frozen spin degree of freedom has also been achieved experimentally.[10] Hence, one can be hopeful that we can study experimentally Bosons with spin in an optical lattice in the Mott regime, where though there is no net mass transport possible, the spin degree of freedom is still active. Due to the finite tunneling amplitude and hence exchange interaction between bosons on neighboring sites, one again expect the possibility of studying quantum magnetism and ordering in these systems. Moreover, it can easily be seen that the spin Hamiltonian realized in these systems would be very different from their counterpart in solid state magnetic systems. For example, for spin-1 atoms, the Hamiltonian coupling neighboring spins $\mathbf{S}_{i,j}$ is of the form [11, 12] $J(\mathbf{S}_i \cdot \mathbf{S}_j) + K(\mathbf{S}_i \cdot \mathbf{S}_j)^2$ with K of the same order as J . This is very different from the usual Heisenberg Hamiltonian $J(\mathbf{S}_i \cdot \mathbf{S}_j)$ which well describes electronic spin interaction in solids. Indeed, a large number of theoretical papers have already been devoted to the subject of the spin physics in these systems. (see [13, 14, 15, 16, 17, 18]

and references therein).

In this paper, we consider spin-1 Bosons in an isotropic three-dimensional optical lattice in the Mott regime of one particle per site. We are in particular interested in the case of anti-ferromagnetic interaction between the atoms, as in the case ^{23}Na . The Hamiltonian [11, 12] correspond to $J < 0$, $K < 0$ with $|J| < |K|$. This spin Hamiltonian has already been considered in the literature even before the field of cold atoms [19, 20]. A general consensus was that, at low temperatures, the system would order in a nematic state which breaks rotational symmetry but has no net spin on any site. (The dimer state, the ground state in one-dimension [11, 15], is unstable towards the nematic state with sufficiently strong coupling between neighboring chains [16]). However, there are some issues in cold-atom systems which were not considered in these works, and we would like to remedy a few of these in this paper. One is the existence of finite magnetic fields in realistic experiments. This magnetic field produces a "quadratic Zeeman" effect[21], which lifts the energy degeneracy between two atoms in the $m_f = 0$ hyperfine sublevel versus one each in $m_f = \pm 1$. The other consideration is that, in the time scale of the experiment, the net "magnetization", namely the sum of m_f over all the particles, is conserved. This "constant magnetization" constraint was usually ignored in previous studies. Since in particular the nematic state itself carries no magnetization, it is natural to ask what is the thermodynamical state of the system if one is constrained to have a finite net magnetization. Besides intrinsic interest, this issue may be relevant since a realistic experiment may not always have exactly equal numbers of $m_f = \pm 1$ atoms in its initial preparation. Lastly, one need to consider finite temperatures. The nematic state can now tolerate some net magnetization via thermally excited particles, and it is of interest to know what this amount would be.

In a previous paper [22], we have already considered the finite temperature thermodynamical properties of the nematic state, but without the effect of finite magnetization and quadratic Zeeman field. There we in particular

have evaluated the entropy of the system, and showed that the nematic state can tolerate a large entropy without being disordered. Since it is now routine that Bose-Einstein condensates be cooled to very low temperatures, it should therefore be relatively easy to reach this nematic state by ramping up an optical lattice from a Bose-Einstein condensate. We are therefore particularly hopeful that physics of the mentioned spin Hamiltonian can be studied in the cold-atom systems.

For the reader's convenience, the different phases concluded in this paper are pictorially shown in Fig. 1 for zero temperature and in Fig. 2 for finite temperatures. At zero temperature, the phases depend on the ground states. For larger magnitude Q of the quadratic Zeeman effect (we shall provide the condition how large Q should be in the main text), only two kinds of states appear: the nematic (NM) state with zero magnetization per site m and the fully magnetic (FM) state with $m = 1$, as shown in Fig. 1(a). In between the two states coexist and are spatially separated. For smaller magnitude Q the two states remain for $m = 0$ (NM) and $m = 1$ (FM), however, a new state appears above the magnetization m_{min} : the partially magnetic (PM) state, as shown in Fig. 1(b). This new state breaks the rotational symmetry along z axis and has magnetization smaller than 1. If the magnetization is between zero and m_{min} , there coexist the NM state and the PM state. For finite temperature, the phase pictures are slightly changed as shown in Fig. 2. The system is not a pure state anymore, but a statistical mixture of different states. For larger Q , we have the NM phase if the net magnetization in the system is between 0 and a small value m_1 , while the FM phase is obtained if $m_2 \leq m \leq 1$. In between, phase separation of NM and FM phases is expected. This is shown in Fig. 1(a). On the other hand, if Q is small, the PM phase will appear as at zero temperature. The NM phase appears with very small magnetization $m \leq m_1$. The PM phase appears spatially separated from NM above m_1 and occupies an increasing volume fraction with increasing magnetization. When m_{min} reached, the PM phase occupies all the region. Above m_2 , the system is in the FM phase.

Our paper is organized as follows. In section II the model for a strongly repulsive atom-atom interaction in an optical lattice with linear and quadratic Zeeman effects is introduced. In section III we provide a mean-field treatment to solve the problem. In section IV the phase diagrams are obtained either as a function of magnitude of linear Zeeman effect or as a function of the magnetization, both at zero temperature (IV A) and at finite temperatures (IV B). In section V some additional discussions and the conclusion are made.

II. MODEL

In this paper, we consider spin-1 Bosons loaded in an strong optical lattice under the influence of linear and

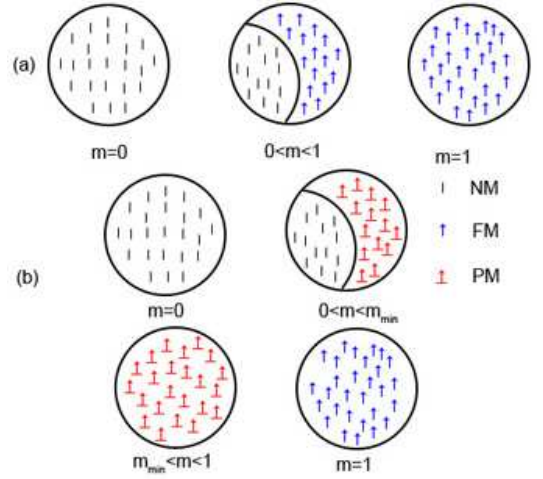


FIG. 1: (color online) Phase pictures for zero temperature. $|$ shows the nematic (NM) state, \uparrow the fully magnetic (FM) state and $\uparrow\downarrow$ the partially magnetic (PM) state. (a) For larger Q . $m = 0$: the NM phase; $0 < m < 1$: NM and FM phases coexist and are spatially separated. $m = 1$: the FM state. (b) For small Q . $m = 0$: NM; $0 < m < m_{min}$: NM and PM, phase separation; $m_{min} < m < 1$: PM and $m = 1$: FM.

quadratic Zeeman effects. In the case of one atom per potential well, such systems can be described by the Hamiltonian

$$H = \sum_{\langle i,j \rangle} H_{ij} + \sum_i \left(H_i^L + H_i^Q \right), \quad (1)$$

where the two-body Hamiltonian H_{ij} is related to Bose Hubbard model and $\langle i, j \rangle$ denotes the next-neighbor sites. Defining the hopping constant t and the interaction strength U_S depending on the total spin $S = 0, 2$, the on-site repulsion coefficients in Bose Hubbard model, the energy of the two-body system can be classified according to the total spin and therefore H_{ij} can be written as [11, 12, 22]

$$H_{ij} = e_0 P_{ij}^{(0)} + e_2 P_{ij}^{(2)} \quad (2)$$

where $e_0 = -\frac{4t^2}{U_0}$, $e_2 = -\frac{4t^2}{U_2}$ and the projection operators $P_{ij}^{(S)}$ project the pair i, j into a total spin hyperfine spin S state. The H_i^L term results from magnetization conservation and the linear Zeeman splitting[21]

$$H_i^L = -\lambda (n_{\uparrow,i} - n_{\downarrow,i}) \quad (3)$$

and H_i^Q is quadratic Zeeman Hamiltonian

$$H_i^Q = 4Q (n_{\uparrow,i} + n_{\downarrow,i}) \quad (4)$$

with n_{\uparrow}, n_0 and n_{\downarrow} representing the number operators with $S_z = 1, 0, -1$, respectively. The two-body Hamiltonian H_{ij} can also be written in a spin representation [11, 12]

$$H_{ij} = J(\mathbf{S}_i \cdot \mathbf{S}_j) + K(\mathbf{S}_i \cdot \mathbf{S}_j)^2 + J - K, \quad (5)$$

where $J = e_2/2$, $K = (2e_0 + e_2)/6$.

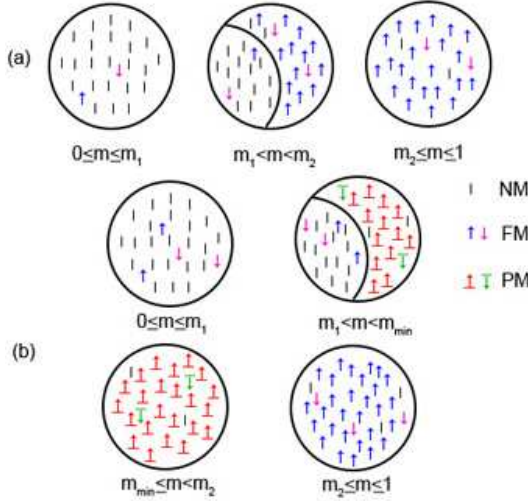


FIG. 2: (color online) Phase pictures for finite temperatures. Different symbols are shown. $|$: NM. \uparrow : FM with positive magnetization. \downarrow : FM with negative magnetization. $\uparrow\cdot$: PM with positive magnetization. $\downarrow\cdot$: PM with negative magnetization. (a) For large Q and (b) for small Q . They are quite similar to the zero-temperature case as shown in Fig. 1. However, there still exist some differences. At finite temperature, the system is composed of statistically mixed states, for example, the NM phase consists of mostly NM states and but mixed with small amounts of FM states. The PM phase consists of large amounts of PM states and small amounts of NM states, *etc.*. The second difference is that the NM and FM phase have a range of magnetization due to this statistical mixture.

III. MEAN-FIELD TREATMENT

As we have mentioned in our recent paper[22], in order to describe the broken $O(3)$ symmetry for nematic state, one can define a new set of basis,

$$\begin{aligned} |x\rangle &= \frac{1}{\sqrt{2}}(-|\uparrow\rangle + |\downarrow\rangle), \\ |y\rangle &= \frac{i}{\sqrt{2}}(|\uparrow\rangle + |\downarrow\rangle), \\ |z\rangle &= |0\rangle \end{aligned} \quad (6)$$

$$(7)$$

In this basis, the two-body Hamiltonian H_{ij} can be expressed as a sum of zero order and second order polynomials

$$\begin{aligned} H_{ij} &= e_0 P_{ij}^{(0)} + e_2 P_{ij}^{(2)} \\ &= \frac{e_0}{3} \sum_{\alpha, \beta=x, y, z} |\alpha\rangle_i \langle \alpha|_{ji} \langle \beta|_j \langle \beta| + e_2 \sum_{\{I\}} |I\rangle \langle I|, \end{aligned} \quad (8)$$

where $|I_{\alpha\beta}\rangle = \frac{1}{\sqrt{2}}(|\alpha\rangle_i |\beta\rangle_j + |\beta\rangle_i |\alpha\rangle_j)$ for $\alpha \neq \beta$, $|I_0\rangle = \sqrt{\frac{2}{3}}(|z\rangle_i |z\rangle_j - \frac{1}{2}|x\rangle_i |x\rangle_j - \frac{1}{2}|y\rangle_i |y\rangle_j)$ and $|I_1\rangle = \frac{1}{\sqrt{2}}(|x\rangle_i |x\rangle_j - |y\rangle_i |y\rangle_j)$, and the linear and quadratic Zeeman

Hamiltonian have the form

$$H_i^L = -i\lambda(|y\rangle_{ii}\langle x| - |x\rangle_{ii}\langle y|), \quad (9)$$

$$H_i^Q = 4Q(|x\rangle_{ii}\langle x| + |y\rangle_{ii}\langle y|). \quad (10)$$

Without H^L and H^Q terms, we have seen [22] that the density matrix should have the diagonalized form $\sum_{\alpha=x, y, z} \rho^{\alpha\alpha} |\alpha\rangle \langle \alpha|$. This obviously remains valid when H^Q is included. However, we see that H^L contains off-diagonal terms in the $|x\rangle, |y\rangle$ representation. Therefore the general density matrix of a single site should have the form

$$\hat{\rho} = \sum_{\alpha=x, y, z} \rho^{\alpha\alpha} |\alpha\rangle \langle \alpha| + \rho^{xy} |x\rangle \langle y| + \rho^{yx} |y\rangle \langle x|, \quad (11)$$

where $\rho^{\alpha\alpha}$ are real and $(\rho^{xy})^* = \rho^{yx}$ due to the hermiticity of $\hat{\rho}$. In this way ρ^{xy} and ρ^{yx} can be chosen purely imaginary because together with ρ^{xx} and ρ^{yy} the real part of ρ^{xy} and ρ^{yx} forms a real symmetric matrix and therefore can be diagonalized. In other words, one can rotate the system along z -axis to make $\rho^{xy} = -\rho^{yx} = -i\rho^{\parallel}$ with real number ρ^{\parallel} .

The principle of mean field theory is to reduce a many-body problem to a one-body problem by replacing all interactions to any one body with an average of effective interaction. A mean-field treatment for a spin-1 Bosons in a lattice has been done by different authors [19, 22]. For Hamiltonian (1), the only term which has to be averaged is the two-body Hamiltonian H_{ij} . The effective Hamiltonian to replace H_{ij} be a single site operator

$$H_{eff}^0 = z \text{Tr}_j [\hat{\rho}_j H_{ij}] = z \text{Tr}_j [\hat{\rho}_j (e_0 P_{ij}^{(0)} + e_2 P_{ij}^{(2)})], \quad (12)$$

with the coordinate number z . For a cubic three-dimensional lattice, $z = 6$. Using Eqs.(8) and (11), H_{eff}^0 can be obtained as

$$\begin{aligned} H_{eff}^0 &= z \sum_{\alpha=x, y, z} (K \rho^{\alpha\alpha} + \frac{e_2}{2}) |\alpha\rangle \langle \alpha| \\ &+ z(2J - K) \{\rho^{xy} |x\rangle \langle y| + \rho^{yx} |y\rangle \langle x|\}. \end{aligned} \quad (13)$$

The total effective Hamiltonian H_{eff} has to include the linear and quadratic Zeeman effect as well

$$\begin{aligned} H_{eff} &= H_{eff}^0 + H^L + H^Q \\ &= H_{eff}^0 - i\lambda \{|y\rangle \langle x| - |x\rangle \langle y|\} \\ &+ 4Q \{|x\rangle \langle x| + |y\rangle \langle y|\}. \end{aligned} \quad (14)$$

Defining a new set of parameters $h^{\alpha\beta}$ as

$$H_{eff} \equiv - \sum_{\alpha=x, y, z} h^{\alpha\alpha} |\alpha\rangle \langle \alpha| - h^{xy} |x\rangle \langle y| - h^{yx} |y\rangle \langle x|, \quad (15)$$

and comparing Eq. (15) with Eqs.(13) and (14) we obtain

$$\begin{aligned} h^{xx} &= -z(K\rho^{xx} + \frac{e_2}{2}) - 4Q \\ h^{yy} &= -z(K\rho^{yy} + \frac{e_2}{2}) - 4Q \\ h^{zz} &= -z(K\rho^{zz} + \frac{e_2}{2}) \\ h^{xy} &= z(K - 2J)\rho^{xy} - i\lambda \equiv -ih^{\parallel} \\ h^{yx} &= -h^{xy}. \end{aligned} \quad (16)$$

where

$$h^{\parallel} \equiv z(K - 2J)\rho^{\parallel} + \lambda \quad (17)$$

and all other components are zero. $h^{\alpha\beta}$ can be one-to-one mapped into $\rho^{\alpha\beta}$ and therefore we can use $h^{\alpha\beta}$ as parameters to find self-consistent equations for the mean-field theory.

To find the self-consistent equations we first rewrite H_{eff} in a matrix representation in $(|x\rangle, |y\rangle, |z\rangle)^T$ basis. H_{eff} therefore has the form

$$H_{eff} = - \left(\sum_{i=0}^3 h_i \sigma_i + h_z \tau_z \right) \quad (18)$$

where

$$\begin{aligned} \sigma_0 &= \begin{bmatrix} 1 & 0 & 0 \\ 0 & 1 & 0 \\ 0 & 0 & 0 \end{bmatrix} & \sigma_1 &= \begin{bmatrix} 0 & 1 & 0 \\ 1 & 0 & 0 \\ 0 & 0 & 0 \end{bmatrix} & \sigma_2 &= \begin{bmatrix} 0 & -i & 0 \\ i & 0 & 0 \\ 0 & 0 & 0 \end{bmatrix} \\ \sigma_3 &= \begin{bmatrix} 1 & 0 & 0 \\ 0 & -1 & 0 \\ 0 & 0 & 0 \end{bmatrix} & \tau_z &= \begin{bmatrix} 0 & 0 & 0 \\ 0 & 0 & 0 \\ 0 & 0 & 1 \end{bmatrix} \end{aligned} \quad (19)$$

and

$$\begin{aligned} h_0 &= \frac{h^{xx} + h^{yy}}{2}, \quad h_1 = 0, \quad h_2 = h^{\parallel}, \\ h_3 &= \frac{h^{xx} - h^{yy}}{2}, \quad h_z = h^{zz}. \end{aligned} \quad (20)$$

For the convenience of latter use, we can also define ρ_i and ρ_z in the same way

$$\begin{aligned} \rho_0 &= \frac{\rho^{xx} + \rho^{yy}}{2}, \quad \rho_1 = 0, \quad \rho_2 = \rho^{\parallel}, \\ \rho_3 &= \frac{\rho^{xx} - \rho^{yy}}{2}, \quad \rho_z = \rho^{zz}. \end{aligned} \quad (21)$$

The one-body density matrix of canonical ensemble is defined as

$$\hat{\rho} = \frac{\exp(-\beta H_{eff})}{\text{Tr} \exp(-\beta H_{eff})} \quad (22)$$

where $\beta \equiv 1/k_B T$. Inserting Eqs.(18), (19) and (20) into Eq. (22) and after some algebra (see Appendix A), $\hat{\rho}$ reads

$$\hat{\rho} = \rho_0 \sigma_0 + \rho_2 \sigma_2 + \rho_3 \sigma_3 + \rho_z \tau_z \quad (23)$$

where

$$\begin{aligned} \rho_0 &= \frac{\cosh \beta h}{e^{\beta h_{zo}} + 2 \cosh \beta h}, \quad \rho_2 = \frac{h_2 \sinh \beta h}{h(e^{\beta h_{zo}} + 2 \cosh \beta h)} \\ \rho_3 &= \frac{h_3 \sinh \beta h}{h(e^{\beta h_{zo}} + 2 \cosh \beta h)}, \quad \rho_z = \frac{e^{\beta h_{zo}}}{(e^{\beta h_{zo}} + 2 \cosh \beta h)} \end{aligned} \quad (24)$$

with the definitions: $h \equiv \sqrt{h_2^2 + h_3^2}$ and $h_{zo} \equiv h_z - h_0$.

Comparing Eq. (16) with Eq. (23), one can obtain three self-consistent equations through the definition of h_{zo} , h_2 and h_3 in Eq. (20). The first equation can be obtained by the relation $h_{zo} = -zK(\rho_z - \rho_0) + 4Q$, which leads to

$$h_{zo} = z|K| \left[\frac{e^{\beta h_{zo}} - \cosh \beta h}{e^{\beta h_{zo}} + 2 \cosh \beta h} \right] + 4Q. \quad (25)$$

$h_2 (= z(K - 2J)\rho_2 + \lambda)$ accounting for the off-diagonal term in the effective Hamiltonian gives the second equation

$$h_2 = z(K - 2J) \frac{h_2 \sinh \beta h}{h(e^{\beta h_{zo}} + 2 \cosh \beta h)} + \lambda. \quad (26)$$

The third equation can be found by the relation: $h_3 = z|K|\rho_3$, which gives the form

$$h_3 = h_3 z|K| \frac{\sinh \beta h}{h(e^{\beta h_{zo}} + 2 \cosh \beta h)}. \quad (27)$$

Therefore there are two situations: if h_3 is nonzero, then Eq. (27) can be reduced to

$$\frac{h}{z|K|} = \frac{\sinh \beta h}{(e^{\beta h_{zo}} + 2 \cosh \beta h)}. \quad (28)$$

Inserting Eq. (28) into Eq. (26), h_2 is a constant

$$h_2 = \frac{|K|\lambda}{2\Delta} \quad (29)$$

with the definition: $\Delta = J - K > 0$. In the case that $h_3 = 0$, $h = h_2$ and Eq.(26) is also reduced to a two parameter equation

$$h_2 = z(K - 2J) \frac{h_2 \sinh \beta h_2}{h(e^{\beta h_{zo}} + 2 \cosh \beta h_2)} + \lambda. \quad (30)$$

In either case we have reduced the mean-field problem to two self-consistent equations.

These self-consistent equations may have many solutions, however, only the one which has the lowest free energy describes the equilibrium state of the system. Therefore we should find the free energy. The free energy can be calculated by the relation

$$F = E_{int} + E_{ext} - TS \quad (31)$$

where the internal energy is given by the two-body interactions $E_{int} = \frac{1}{2} \text{Tr} \hat{\rho} H_{eff}^0$ and the external energy

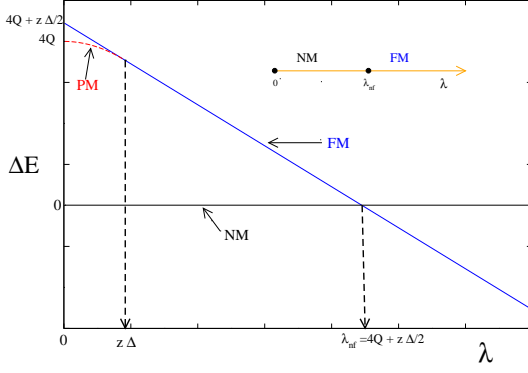


FIG. 3: (color online) Energy difference of the NM, FM and PM states with respect to the NM state vs. λ for $4Q > z\Delta/2$. The black line shows the reference state: NM, the blue line shows the FM state and red-dashed line shows the PM state. $\lambda_{n,f}$ is the point of a first order phase transition. In the inset we show the phase diagram in terms of λ .

is given by the Zeeman fields $E_{ext} = \text{Tr} \hat{\rho} \{H^L + H^Q\}$. After some algebra (see Appendix B) the free energy is obtained as follows:

$$E_{int} = \frac{zK}{2} \left[1 - \frac{4e^{\beta h_{zo}} \cosh \beta h + 2}{(e^{\beta h_{zo}} + 2 \cosh \beta h)^2} \right] + 2z\Delta \frac{h_2^2 \sinh^2 \beta h}{h^2 (e^{\beta h_{zo}} + 2 \cosh \beta h)^2} + \frac{ze_2}{4}, \quad (32)$$

$$E_{ext} = -4Q \frac{e^{\beta h_{zo}}}{e^{\beta h_{zo}} + 2 \cosh \beta h} - 2\lambda \frac{h_2 \sinh \beta h}{h(e^{\beta h_{zo}} + 2 \cosh \beta h)} + 4Q \quad (33)$$

and

$$-TS = \frac{h_{zo} e^{\beta h_{zo}}}{e^{\beta h_{zo}} + 2 \cosh \beta h} + \frac{2h \sinh \beta h}{e^{\beta h_{zo}} + 2 \cosh \beta h} - \frac{1}{\beta} \ln (e^{\beta h_{zo}} + 2 \cosh \beta h). \quad (34)$$

IV. PHASE DIAGRAMS

In the following, we discuss different phases at zero temperature and at finite temperatures.

A. Zero Temperature

At zero temperature, ρ_{eff} is dominated by the smallest eigenvalue of H_{eff} , which can be easily found by diagonalizing Eq. (14). H_{eff} can be rewritten as follows

$$H_{eff} = -h_0 \mathbb{1} - h_2 \sigma_2 - h_3 \sigma_3 - h_{zo} \tau_z \quad (35)$$

with identity matrix $\mathbb{1}$. Obviously $h_0 \mathbb{1}$ is a constant matrix, therefore it can be ignored. We define a new Hamiltonian

$$H_{eff}^n = -h_2 \sigma_2 - h_3 \sigma_3 - h_{zo} \tau_z. \quad (36)$$

One has three eigenvalues for H_{eff}^n : eigenvalue $-h_{zo}$ correspond to eigenvector $[0, 0, 1]^T (|z\rangle)$ and eigenvalues $\pm h$ correspond to eigenvectors: $[u_{\pm}, v_{\pm}, 0]^T$, i.e. $(u_{\pm}|x\rangle + v_{\pm}|y\rangle)$. $u_{-}|x\rangle + v_{-}|y\rangle$ is irrelevant at $T = 0$ because its eigenvalue h is positive. Therefore if $h_{zo} > h$, the system is in the pure nematic state $|z\rangle$, otherwise the system is in the $(u_{+}|x\rangle + v_{+}|y\rangle)$ state. This state can be either a partially magnetic (PM) state or a fully magnetic (FM) state depending on the parameters λ and q . We will discuss the details later.

In the case $h_{zo} > h$, the free energy can be calculated by using Eqs. (31) - (34). We can see that at zero temperature the equations show the competition between h_{zo} and h . After some algebra, F can be rewritten as a function of $\cosh \beta h / e^{h_{zo}}$ and of $\sinh \beta h / e^{h_{zo}}$. These two terms disappear at zero temperature. Therefore

$$F = \frac{zK}{2} + \frac{ze_2}{4} \equiv E_z. \quad (37)$$

We see that $E_z = \frac{zK}{2} + \frac{ze_2}{4} = z(e_0 + 2e_2)/6$ is independent of λ and Q .

On the contrary, if $h > h_{zo}$, the eigenvector of H_{eff}^n can be solved by the equation below

$$(h_2 \sigma_2 + h_3 \sigma_3)(u_{+}|x\rangle + v_{+}|y\rangle) = h(u_{+}|x\rangle + v_{+}|y\rangle). \quad (38)$$

This yields

$$u_{+} = \frac{1}{\sqrt{2}} \left(1 + \frac{h_3}{h} \right)^{\frac{1}{2}}, \quad v_{+} = \frac{ih_2}{\sqrt{2}h} \frac{1}{\left(1 + \frac{h_3}{h} \right)^{\frac{1}{2}}}. \quad (39)$$

In a similar way, by using Eq. (31) - (34), the free energy defined as E_{+} has the form

$$F = \frac{zK}{2} + \frac{ze_2}{4} + \frac{z\Delta}{2} \left(\frac{h_2}{h} \right)^2 - \lambda \frac{h_2}{h} + 4Q \equiv E_{+}. \quad (40)$$

We can define $h_2/h = \cos \theta$ and $h_3/h = \sin \theta$ since $h^2 = h_2^2 + h_3^2$. E_{+} then takes the form

$$E_{+} = \frac{zK}{2} + \frac{ze_2}{4} + \frac{z\Delta}{2} \cos^2 \theta - \lambda \cos \theta + 4Q. \quad (41)$$

There are two minima for E_{+} : either

$$\sin \theta = 0 \quad (42)$$

or

$$\cos \theta = \frac{\lambda}{z\Delta}. \quad (43)$$

The second solution has a constraint: $\lambda < z\Delta$, otherwise there is no solution due to the fact that $\cos \theta$ can not

be larger than 1. These two saddle points can be also obtained by the self-consistent equations. In the case $h_3 = 0$, this indicates directly that $\sin \theta = 0$. This yields $\theta_0 = 0$ and then $u = \frac{1}{\sqrt{2}}$ and $v = \frac{i}{\sqrt{2}}$ according to Eq. (39). Therefore the ground state reads

$$|\Psi\rangle = \frac{1}{\sqrt{2}}(|x\rangle + i|y\rangle) = -|\uparrow\rangle. \quad (44)$$

Therefore we obtain a fully magnetic (FM) state. On the contrary, if $h_3 \neq 0$ at $T = 0$, Eq. (28) is reduced to the form

$$h = \frac{z|K|}{2}. \quad (45)$$

Together with Eq. (29), we obtain Eq. (43). The eigenstate of this solution is

$$|\Psi\rangle = u|x\rangle + v|y\rangle \quad (46)$$

where $u, v (\neq \pm 1)$ are given by Eq. (39). Transforming the state into spin basis, we obtain a state :

$$|\Psi\rangle = \alpha|\uparrow\rangle + \gamma|\downarrow\rangle \quad (47)$$

where

$$\alpha = \frac{-u + iv}{\sqrt{2}} = -\frac{1}{\sqrt{2}}\sqrt{1 + \frac{h_2}{h}} \neq 0 \quad (48)$$

and

$$\gamma = \frac{u + iv}{\sqrt{2}} = \frac{1}{\sqrt{2}}\sqrt{1 - \frac{h_2}{h}} \neq 0 \quad (49)$$

by using Eq. (39). We call this a partially magnetic (PM) state. We note that $h_3 \neq 0$ implies that x and y axes are no longer equivalent and the rotational symmetry about the z -axis is spontaneously broken in this PM state.

We can summarize that we have three phases: nematic state (NM) $|z\rangle$, FM state $|\uparrow\rangle$ and PM state $\alpha|\uparrow\rangle + \gamma|\downarrow\rangle$. To see which state is preferred we have to calculate the free energy for these three states. Define the energy difference first : $\Delta E \equiv E_+ - E_z$. This yields

$$\Delta E(\theta) = \frac{z\Delta}{2}(\cos \theta)^2 - \lambda \cos \theta + 4Q. \quad (50)$$

Therefore a FM state has the energy difference to a NM state

$$\Delta E(\theta_0) = \frac{z\Delta}{2} + 4Q - \lambda, \quad (51)$$

while a PM state has the energy difference

$$\Delta E(\theta_1) = 4Q - \frac{\lambda^2}{2z\Delta} \quad (52)$$

with the constraint: $\lambda < z\Delta$. A state is favored over the NM states only if $\Delta E < 0$. Therefore a PM state can be a ground state if there exists a critical lambda $\lambda_{n,p}$

$$\lambda_{n,p} = \sqrt{8Qz\Delta} \quad (53)$$

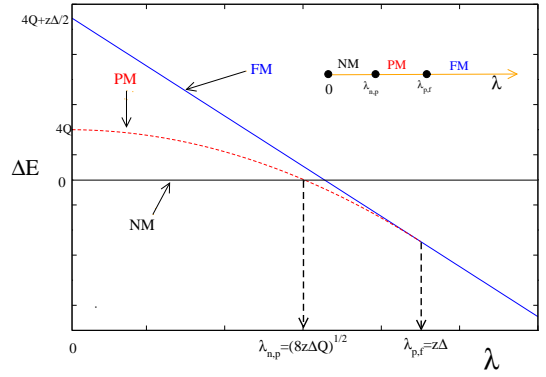


FIG. 4: (color online) Energy difference of the NM, FM and PM states with respect to the NM state vs. λ for $0 < 4Q < z\Delta/2$. The black line shows the reference state: NM, the blue line shows the FM state and red-dashed line shows the PM state. $\lambda_{n,p}$ is the point that a first order phase transition occurs from NM to PM and $\lambda_{p,f}$ is the second-order phase-transition point from PM to FM. In the inset we show the phase diagram in terms of λ .

where $\lambda_{n,p} < z\Delta$. That means a PM state can be a ground state only with the condition

$$4Q < \frac{z\Delta}{2}. \quad (54)$$

This separates the whole parameter space into two regimes: a regime with PM states and a regime without.

(a) $4Q \geq \frac{z\Delta}{2}$: In this regime, there exist only two states: NM and FM. Fig. 3 shows ΔE of different states. Since we subtract the energy of the nematic state in the definition of ΔE , we can define $\Delta E = 0$ for the nematic state, as the black line shown in Fig. 3. The blue line decreasing linearly shows $\Delta E(\theta_0)$, the energy difference for FM (51). $\Delta E(\theta_0)$ becomes negative if $\lambda < \lambda_{n,f}$, where

$$\lambda_{n,f} = 4Q + \frac{z\Delta}{2}. \quad (55)$$

The system undergoes a first-order phase transition from nematic states to fully magnetic states while λ passing $\lambda_{n,f}$. This picture is also drawn in Fig. 3. The reason why the phase transition is first-order is that the magnetization jumps from zero for nematic states to one for ferromagnetic states. We note that from Eq. (3) $\partial \Delta E / \partial \lambda = -(n_\uparrow - n_\downarrow)$, hence the slope of ΔE versus λ is proportional to the magnetization. In order to see that the PM state does not appear in this regime, we also draw $\Delta E(\theta_1)$ as the red line in Fig. 3. $\Delta E(\theta_1)$ is always positive till the end point $\lambda = z\Delta$. Therefore PM never appears in this regime.

In experiments the magnetization is constant in time, therefore it is important to have a phase diagram with magnetization as a parameter. Supposed that average magnetization per site is m , the system is purely NM only if $m = 0$, while it is purely FM only if $m = 1$. In between

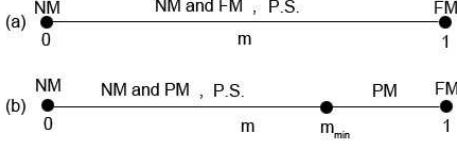


FIG. 5: (color online) Phase diagrams for zero Temperature in terms of average net magnetization m . (a) $4Q > z\Delta/2$ (b) $0 < 4Q < z\Delta/2$. P.S. means phase separation. This figure corresponds to Fig. 1.

we have phase separation since the phase transition is first-order. If x is the fraction of nematic state, then $x = 1 - m$. This phase diagram is drawn in Fig.5 (a).

(b) $0 < 4Q < \frac{z\Delta}{2}$: Fig 4 shows ΔE for different states. $\Delta E(\theta_1)$ is shown with a red dashed line, while $\Delta E(\theta_0)$ with a blue line as in Fig. 3. We can see that the red dashed line crosses zero at $\lambda_{n,p}$ defined as (53) and then merges to the blue line at the point

$$\lambda_{p,f} \equiv z\Delta. \quad (56)$$

In the regime: $0 < \lambda < \lambda_{n,p}$ the ground state is nematic, for $\lambda_{n,p} < \lambda < \lambda_{p,f}$ the system is partially magnetic and one has a fully magnetic state if $\lambda > \lambda_{p,f}$. Therefore the system undergoes two phase transitions: a first-order phase transition from NM to PM at $\lambda_{n,p}$ and a second-order phase transition from PM to FM at $\lambda_{p,f}$. The second phase transition is second order due to the fact that θ_1 goes to zero while λ approaching $z\Delta$, and therefore the transition is continuous for the order parameter. This yields the phase diagram in the inset of Fig. 4.

The same question arises: if we have a net averaged magnetization per site m , which state we will achieve. To see this, we have to calculate the net magnetization for the PM state. From Eq.(47), (48) and (49) we can calculate m

$$m = |\alpha|^2 - |\gamma|^2 = \frac{h_2}{h}, \quad (57)$$

which leads to

$$m = \frac{h_2}{h} = \cos \theta_1 = \frac{\lambda}{z\Delta} \quad (58)$$

by using Eq. (43). Therefore in the regime of PM states, $\lambda_{n,p} < \lambda < \lambda_{p,f}$, the magnetization lies in the region

$$\sqrt{\frac{8Q}{z\Delta}} < m < 1. \quad (59)$$

The PM state has a minimum magnetization

$$m_{min} = \sqrt{\frac{8Q}{z\Delta}}. \quad (60)$$

As a result, if $m = 0$, the system is purely nematic. For $0 < m < m_{min}$ phase separation occurs. One has

the nematic state and the PM state spatially separated. Supposed that the fraction in nematic state is defined as x , we obtain $x = 1 - m\sqrt{\frac{z\Delta}{8Q}}$. In the regime: $m_{min} < m < 1$, PM covers the entire system and there exists no nematic state. Finally, if $m = 1$, we obtain FM again. These results are shown in Fig.5 (b).

We remark here that the phase diagrams in the inset of Fig. 4 and Fig. 5 are analogous to the superfluid case given in Ref.[4]. In mean field theories both the lattice and superfluid cases yield mean field energy of the same forms due to symmetry.

B. Finite Temperature

Before we determine the phase diagram for finite temperature, we first figure out different phases by investigating eigenstates of the density matrix $\hat{\rho}$ (11). After diagonalizing it, $\hat{\rho}$ is in its diagonalized form

$$\hat{\rho} = P_+|\Psi_+\rangle\langle\Psi_+| + P_-|\Psi_-\rangle\langle\Psi_-| + P_z|z\rangle\langle z|, \quad (61)$$

where

$$P_{\pm} = \rho_0 \pm \sqrt{\rho_2^2 + \rho_3^2}, \quad P_z = \rho_z. \quad (62)$$

The eigenvectors read

$$|\Psi_{\pm}\rangle = u_{\pm}|x\rangle + v_{\pm}|y\rangle, \quad (63)$$

where

$$\begin{aligned} u_+ &= v_- = \frac{D}{\sqrt{D^2 + \rho_2^2}} \\ u_- &= v_+ = \frac{i\rho_2}{\sqrt{D^2 + \rho_2^2}} \end{aligned} \quad (64)$$

with the definition:

$$D = \rho_3 + \sqrt{\rho_2^2 + \rho_3^2}. \quad (65)$$

In order to obtain the true phases we have to solve the self-consistent equations Eqs. (25) to Eqs. (30). As discussed in the last section, one can categorize these self-consistent equations into two groups: (1) $h_3 = 0$ and (2) $h_3 \neq 0$ with a constant h_2 . In the case $h_3 = 0$, $\rho_{xx} = \rho_{yy}$ (i.e. $h_3 = 0$), the eigenvalues (62) reads

$$P_{\pm} = \rho_0 \pm \rho_2 = \rho_{xx} \pm |\rho_{xy}|. \quad (66)$$

According to Eq. (64), $u_+ = v_- = \frac{1}{\sqrt{2}}$ and $u_- = v_+ = \frac{i}{\sqrt{2}}$, $|\Psi_+\rangle$ thus has the form

$$|\Psi_+\rangle = \frac{1}{\sqrt{2}}(|x\rangle + i|y\rangle) = -|\uparrow\rangle, \quad (67)$$

while $|\Psi_-\rangle$ reads

$$|\Psi_-\rangle = \frac{i}{\sqrt{2}}(|x\rangle - i|y\rangle) = i|\downarrow\rangle. \quad (68)$$

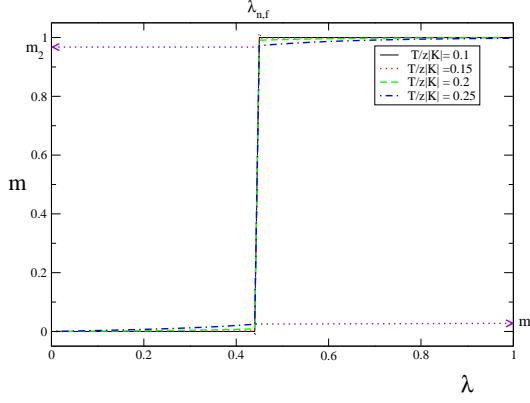


FIG. 6: (color online) The average magnetization per site m vs. λ for different temperatures. The parameters: $Q/z|K| = 0.1$, $J/K = 0.91$, $\Delta = 0.1|K|$. We can see that there is a huge magnetization jump at $\lambda_{n,f} (\simeq 0.446)$ even for $T/z|K| = 0.25$. The maximum magnetization in NM is m_1 and the minimum magnetization in FM is m_2 .

Therefore the system is a mixed state of $|\uparrow\rangle$, $|\downarrow\rangle$ and $|z\rangle$.

In the second case that $h_3 \neq 0$ and $h_2 = \text{const.}$, the eigenstate $|\Psi_+\rangle$ can be rewritten as

$$|\Psi_+\rangle = \alpha|\uparrow\rangle + \gamma|\downarrow\rangle \quad (69)$$

where

$$\alpha = -\frac{1}{\sqrt{2}}(u_+ - iv_+), \quad \gamma = \frac{1}{\sqrt{2}}(u_+ + iv_+). \quad (70)$$

α, γ are nonzero real numbers and $\alpha \neq \gamma$. Similarly, $|\Psi_-\rangle$ has the form

$$|\Psi_-\rangle = -\gamma|\uparrow\rangle + \alpha|\downarrow\rangle. \quad (71)$$

We can easily prove that $|\Psi_+\rangle$ is orthonormal to $|\Psi_-\rangle$. The system is a mixed state with $(\alpha|\uparrow\rangle + \gamma|\downarrow\rangle), (-\gamma|\uparrow\rangle + \alpha|\downarrow\rangle)$ and $|z\rangle$.

Numerically we solved the self-consistent equations and calculated their free energy according to Eqs. (31), (32), (33) and (34). $J/K = 0.91$ has been used to be close to those for ^{23}Na . In this case $\Delta = 0.091|K|$. In order to find the convergent solution quickly, we start with low temperature ($T/z|K| = 0.1$) and extends the temperature step by step by using the final results as an initial input for the next temperature. We have evaluated the phase diagram up to $T/z|K| = 0.25$. We note that if $\lambda = Q = 0$, the nematic state becomes disordered at $T/z|K| \simeq 0.36$. We illustrate our result with two Q values: $Q/z|K| = 0.1$ and $Q/z|K| = 0.005$ to represent two regimes as for Fig. 3 and Fig. 4. We separate the two sets of self-consistent solutions: one with $h_3 = 0$ and one with $h_3 \neq 0$ and $h_2 = \text{const.}$. For the set of zero h_3 , two subsets occur. The first one contains the points with small h_2 : $h_2 \ll 1$ and h_2 of the second subset is of order 1. Compared with the solutions of zero temperature, the first subset is a continuous evolution with the temperature T from the nematic solution, therefore we can

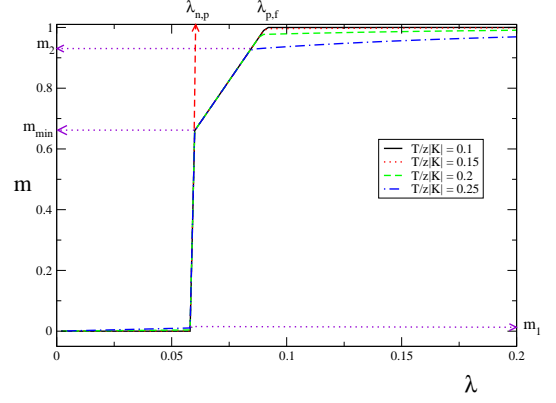


FIG. 7: (color online) The average magnetization per site m vs. λ for different temperatures. $Q/z|K| = 0.005$ and other parameters are same as Fig. 6. m_{\min} is the minimum magnetization at which PM exists. A first-order phase transition occurs at $\lambda_{n,p} \simeq 0.06$ from NM to PM and a second-order phase transition occurs at $\lambda_{p,f}$ depending on the temperature.

still call these solution nematic (NM), while in case of large h_2 the solutions correspond to the fully magnetic states (FM) at zero temperature. On the other hand, if $h_3 \neq 0$ and $h_2 = \text{const.}$, the states we obtain evolve from the PM states at zero temperature, we can still call them partially magnetic.

(a) $Q/z|K| = 0.1$: in this case, we can calculate the free energy vs. λ for the three different sets discussed above. The result is very similar to Fig. 3 for each temperature except that the free energy for nematic phase is not constant anymore but a monotonic decreasing function of λ . The transition points $\lambda_{n,f}$ of the first order phase transition stay almost the same for all temperatures, for this Q , $\lambda_{n,f} \simeq 0.446$. The nematic phase at finite temperatures is not a pure state anymore, it contains mostly the nematic state $|z\rangle$ and with small amounts of $|\uparrow\rangle$ and $|\downarrow\rangle$ due to the fact that $0 \neq h_2 \ll 1$. Therefore the magnetization is not zero. On the other hand, the FM phase is a mixture of large amount of $|\uparrow\rangle$ and small amounts of $|\downarrow\rangle$ and $|z\rangle$, as a result, the magnetization is smaller than one. PM phase can not appear here.

We can also calculate magnetization for NM and FM phases by the relation

$$m = \text{Tr}(n_\uparrow - n_\downarrow)\hat{\rho}. \quad (72)$$

It yields $m = 2\rho_2$. Fig. 6 shows the magnetization at different temperatures in terms of λ . m increases monotonically till it reaches its maximum m_1 at $\lambda_{n,f}$ and then jumps to value m_2 . At the end it increases to the fully magnetic state $m = 1$ if $\lambda \gg 1$. At higher temperatures, m_1 increases and m_2 decreases due to the fact that NM and FM mix more and more different states. As a result, if $0 \leq m \leq m_1$, the system can be a uniform NM phase, while $m_2 \leq m \leq 1$, we obtain a uniform FM phase. In between, $m_1 < m < m_2$, NM and FM coexist and they are phase separated since the phase transition is first-

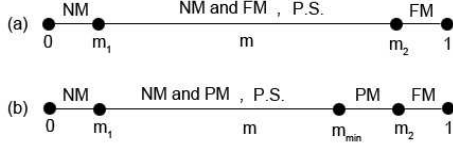


FIG. 8: Phase diagrams for finite temperatures in terms of average net magnetization m . (a) large Q (b) small Q . P.S. means phase separation. This figure corresponds to Fig. 2.

order. We summarize the result in Fig. 8 (a).

(b) $Q/z|K| = 0.005$: similar to the zero temperature case, PM phase appears here. The free energy curves vs. λ for different temperatures are similar to Fig. 4. The first-order phase transition point stays the same: $\lambda_{np} \simeq 0.06$ for all temperatures, while the second-order phase-transition point λ_{pf} changes: $\lambda_{pf} = 0.091, 0.09, 0.088, 0.084$ for $T/z|K| = 0.1, 0.15, 0.2, 0.25$, respectively. The reason is that for PM phase the constraint $h_2 < h$ has to be satisfied, it demands

$$\lambda \leq z\Delta \frac{2 \sinh \beta h}{e^{\beta h_{zo}} + 2 \cosh \beta h} \equiv h_{p,f}(T). \quad (73)$$

At zero temperature, $\lambda_{p,f}(0) = z\Delta$ which agrees with the result we obtained in the last section. With increasing T (decreasing β), $e^{\beta h_{zo}}$ is getting larger, λ_{pf} is thus decreasing.

As discussed above, PM phase has large amount of $(\alpha|\uparrow) + \gamma|\downarrow)$ mixed with small amounts of $(-\gamma|\uparrow) + \alpha|\downarrow)$ and $|z\rangle$. The magnetization of the system for different temperatures as a function of λ is shown in Fig. 7. In NM phase, m increases and then jumps to m_{min} at $\lambda_{n,p}$. The system undergoes a first order phase transition. In PM phase m ascends to m_2 and the system changes continuously to FM phase. We conclude that if $1 \leq m \leq m_1$ a homogeneous NM phase is achievable in experiments. In the case that $m_1 < m < m_{min}$, NM and PM phases coexist but separate spatially. In the regime: $m_{min} < m < m_2$, PM phase with different magnetization is the only phase in the system. In the end, if $m_2 \leq m \leq 1$, we obtain FM phase. The phase diagram is plotted in Fig. 8 (b).

V. DISCUSSION AND CONCLUSION

In the case $\lambda = 0$ and $Q = 0$, there exists a first-order phase transition between the nematic state and the disordered state at $T/z|K| = 0.36$ [22]. The question arises naturally that if Q is nonzero, how the first-order phase transition develops. Fig. 9 shows the density ρ_z as a function of temperature with increasing Q . Note that $\rho_z = 1/3$ corresponds to a state with $O(3)$ symmetry. We found that the first-order phase transition exists till $Q = 0.002z|K|$ (red-dotted line) and then it

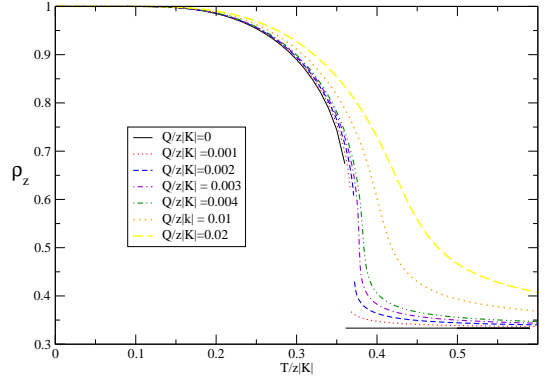


FIG. 9: (color online) ρ_z vs. temperature for different Q 's. In this figure, $\lambda = 0$. The first-order phase transition predicted for $Q = 0$ still exists till $Q = 0.002z|K|$. Even for larger Q , we can still see a rapid decrease of ρ_z when T increases from the low to high temperature regime.

turns to be a sharp crossover even till $Q \simeq 0.02z|K|$ (thick yellow dashed line). From Ref.[4], Q is related to the magnetic field B : $4Q = 278 * B^2 (HzG^{-2})$, that means for $Q = 0.002z|K|$, $B = 0.0134\sqrt{|K|}G$ with Hz as the unit of $|K|$. If the superexchange parameter is $|K| \simeq 100Hz$ [23], this yields $B = 0.134G$. For $Q = 0.02z|K|$, $B = 0.42G$. Experimentally one can reach $B < 0.01G$, therefore the first-order phase transition and the sharp crossover can be observable. On the other hand, as shown in text, the first-order phase transition from the NM state to FM state for large Q and from the NM state to PM state for smaller Q remain at finite temperature. We conclude that these phases would phase separate into different spatial regions. One may ask whether, instead of phase separation, one can have, for example, the ferromagnetic sites appear in the form of linear or planar stripes within the nematic regions. We exclude this for the following reason. According to Eq. (2) and $U_2 \simeq U_0$ for ^{23}Na , we obtain $e_0 \simeq e_2 < e_1 = 0$, where e_1 is the energy for total spin for two atoms equal to 1. Consider two neighboring sites. From the Clebsch-Gordan coefficients we can write down $|0,0\rangle$ as a linear combination of $|F_{tot} = 0\rangle$ and $|F_{tot} = 2\rangle$, and $|1,1\rangle$ only exists in $|F_{tot} = 2\rangle$, while $|1,0\rangle$ and $|0,1\rangle$ must involve the high energy $|F_{tot} = 1\rangle$ state. Therefore it costs more energy if the system builds a domain wall than just put the same m_f state as neighbors. That is the reason why the system prefers a spatially separated phase than stripe phases. A stripe phase is not favored because it needs to build more than one domain wall.

To conclude, we have shown the phase diagrams for a spin-1 polar Bose gas loaded in an strongly repulsive optical lattice. There exist three different phases: the nematic (NM), fully magnetic (PM) and partially magnetic (PM) phases depending on the parameter regime of the system. A first-order phase transition from NM to FM or from NM to PM has been predicted. A second-order phase transition from PM to FM is also found. These

phase transitions are robust even at finite temperatures. Therefore they should be observable in experiments.

APPENDIX A: DENSITY MATRIX

To obtain $\hat{\rho}$ defined as Eq. (22), we have to calculate $e^{-\beta H_{eff}}$ first. It can be written in the form

$$e^{-\beta H} = e^{\beta(\sum_{i=0}^3 h_i \sigma_i + h_z \tau_z)}. \quad (A1)$$

Since τ_z commutes with all σ_i , we can take $e^{\beta h_z \tau_z}$ out of the exponential. One can prove the relation with properties of Pauli matrices:

$$e^{\xi \hat{n} \cdot \sigma} = \cosh \xi + \hat{n} \cdot \sigma \sinh \xi, \quad (A2)$$

where \hat{n} is a three dimensional normal vector and $\sigma = [\sigma_1, \sigma_2, \sigma_3]^T$. By using this, Eq.(A1) has the form

$$e^{-\beta H} = e^{\beta h_z \tau_z} + e^{\beta h_0} \cosh \beta h \sigma_0 + \left(\frac{h_2}{h} \sigma_2 + \frac{h_3}{h} \sigma_3 \right) e^{\beta h_0} \sinh \beta h. \quad (A3)$$

It yields

$$\text{Tr } e^{-\beta H} = e^{\beta h_z} + 2e^{\beta h_0} \cosh \beta h. \quad (A4)$$

Eq. (23) together with Eq. (24) are thus obtained.

APPENDIX B: FREE ENERGY

The internal energy can be calculated by using Eq.(13) as follows

$$\begin{aligned} E_{int} &= \frac{1}{2} \text{Tr } \hat{\rho} H_{eff}^0 \\ &= \frac{1}{2} z \sum_{\alpha=x,y,z} (K \rho^{\alpha\alpha} + \frac{e_2}{2}) \rho^{\alpha\alpha} \\ &\quad + z \left(J - \frac{K}{2} \right) \{ \rho^{xy} \rho^{yx} + \rho^{yx} \rho^{xy} \} \end{aligned} \quad (B1)$$

This term can be simplified to a form

$$E_{int} = \frac{zK}{2} \text{Tr } \hat{\rho}^2 + 2z(J - K) \rho_2^2 + \frac{ze_2}{4}. \quad (B2)$$

Note that $\text{Tr } \hat{\rho}^2 = 2\rho_0^2 + 2\rho_2^2 + 2\rho_3^2 + \rho_z^2$. Inserting Eq. (24) into Eq. (B2), we obtain internal energy as Eq. (32). E_{ext} can be calculated in a similar way:

$$\begin{aligned} E_{ext} &= \text{Tr } \hat{\rho} \{ 4Q(|x\rangle\langle x| + |y\rangle\langle y|) \\ &\quad + i\lambda(|x\rangle\langle y| - |y\rangle\langle x|) \} \\ &= 4Q - 4Q\rho^{zz} - 2i\lambda\rho^{xy}, \end{aligned} \quad (B3)$$

this yields

$$E_{ext} = 4Q - 4Q\rho_z - 2\lambda\rho_2. \quad (B4)$$

Therefore Eq. (33) is obtained by using Eq. (24).

Finally $-TS$ can be obtained by the definition of entropy:

$$S \equiv -k_B \text{Tr } \hat{\rho} \ln \hat{\rho}. \quad (B5)$$

It yields

$$\begin{aligned} -TS &= -\text{Tr } \hat{\rho} H_{eff} - \frac{1}{\beta} \ln \text{Tr } e^{\beta H_{eff}} \\ &= (2\rho_0 - 1)h_0 + 2\rho_2 h_2 + 2\rho_3 h_3 + \rho_z h_z \\ &\quad - \frac{1}{\beta} \ln (e^{\beta h_z} + 2 \cosh \beta h), \end{aligned} \quad (B6)$$

and therefore Eq.(34).

-
- [1] P. A. Lee, N. Nagaosa and X.-G. Wen, Rev. Mod. Phys. **78**, 15 (2006)
 - [2] R. Jördens, N. Strohmaier, K. Günter, H. Moritz and T. Esslinger, Nature (London) **455**, 204 (2008)
 - [3] U. Schneider, L. Hackermüller, S. Will, Th. Best, I. Bloch, T. A. Costi, R. W. Helmes, D. Rasch and A. Rosch, Science, **322**, 1520 (2008)
 - [4] J. Stenger, D.M. Stamper-Kurn, H.J. Miesner, A.P. Chikkatur, W. Ketterle, Nature (London), **396**, 345 (1999).
 - [5] A. T. Black, E. Gomez, L. D. Turner, S. Jung and P. D. Lett, Phys. Rev. Lett. **99**, 070403 (2007); Y. Liu, S. Jung, S. E. Maxwell, L. D. Turner, E. Tiesinga and P. D. Lett, *ibid*, **102**, 125301 (2009).
 - [6] M. S. Chang, C. D. Hamley, M. D. Barrett, J. A. Sauer, K. M. Fortier, W. Zhang, L. You and M. S. Chapman, Phys. Rev. Lett. **92**, 140403 (2004); Nature Phys. **1**, 111 (2005)

- [7] H. Schmaljohann, M. Erhard, J. Kronjäger, M. Kottke, S. van Staa, L. Cacciapuoti, J. J. Arlt, K. Bongs and K. Sengstock, Phys. Rev. Lett. **92** 040402 (2004)
- [8] T. Kuwamoto, K. Araki, T. Eno and T. Hirano, Phys. Rev. A **69**, 063604 (2004)
- [9] A. Griesmaier, J. Werner, S. Hensler, J. Stuhler and T. Pfau, Phys. Rev. Lett. **94**, 160401 (2005)
- [10] M. Greiner, O. Mandel, T. Esslinger, T. W. Hänsch and I. Bloch, Nature, **415**, 39 (2002); T. Stöferle, H. Moritz, C. Schori, M. Köhl and T. Esslinger, Phys. Rev. Lett. **92**, 130403 (2004); G. K. Campbell, J. Mun, M. Boyd, P. Medley, A. E. Leanhardt, L. G. Marcassa, D. E. Pritchard and W. Ketterle, Science, **313**, 649 (2006); S. Fölling, A. Widera, T. Müller, F. Gerbier and I. Bloch, Phys. Rev. Lett. **97**, 060403 (2006); I. B. Spielman, W. D. Phillips and J. V. Porto, *ibid*, **98**, 080404 (2007); T. Fukuhara, S. Sugawa, M. Sugimoto, S. Taie and Y. Takahashi, Phys. Rev. A **79**, 041604 (2009)
- [11] S.-K. Yip, Phys. Rev. Lett. **90**, 250402 (2003)
- [12] A. Imambekov, M. Lukin and E. Demler, Phys. Rev. A **68**, 063602 (2003)
- [13] A. B. Kuklov and B. V. Svistunov, Phys. Rev. Lett. **90**, 100401 (2003); E. Altman, W. Hofstetter, E. Demler and M. D. Lukin, New J. Phys. **5**, 113.1 (2003)
- [14] M. Snoek and F. Zhou, Phys. Rev. B **69**, 094410 (2004)
- [15] M. Rizzi, D. Rossini, G. De Chiara, S. Montangero and R. Fazio, Phys. Rev. Lett. **95**, 240404 (2005)
- [16] K. Harada, N. Kawashima and M. Troyer, J. Phys. Soc. Jpn., **76**, 013703 (2007)
- [17] F. Zhou and G. W. Semenoff, Phys. Rev. Lett. **97**, 180411 (2006); J. L. Song, G. W. Semenoff, and F. Zhou, *ibid*, **98**, 100401 (2007); A. M. Turner, R. Barnett, E. Demler, and A. Vishwanath, *ibid*, **98**, 190404 (2007); J. L. Song and F. Zhou, Phys. Rev. A **77**, 033628 (2008)
- [18] J.-S. Bernier, K. Sengupta and Y. B. Kim, Phys. Rev. B **76**, 014502 (2007)
- [19] H. H. Chen and P. M. Levy, Phys. Rev. B. **7**, 4267 (1973)
- [20] N. Papanicolaou, Nucl. Phys. **B305**, 367 (1988)
- [21] The linear Zeeman field splitting combines with the Lagrange multiplier for the constant magnetization constraint to form the coefficient λ in Eq. (3) and therefore does not yield an additional physical parameter.
- [22] M. C. Chung and S.-K. Yip, arXiv: 0811.2054
- [23] S. Trotzky, *et. al.* Science **319**, 295 (2008).